Electronic Supplementary Materials

Photoanode Immobilized Homogeneous Cobalt-Based Oxygen-Evolving Complexes with Enhanced Solar-to-Fuel Efficiency

*Zhaoyu Jin, Panpan Li and Dan Xiao**

Experimental details

Synthesis of N,N'-5,6-bis(salicylideneimino)-1,10-phenanthroline (PBI). The method was reported in our previous work[1] and described briefly as follows: 1,10-phenanthroline-5,6-diamine (200 mg, 0.95 mmol) and 2-hydroxy-3-methoxybenzaldehyde (578 mg, 3.8 mmol) were suspended in anhydrous ethanol (30 mL) together with a few drops of triethyl orthoformate (~ 0.5 mL) as the dehydrating agent. The mixture was heated to reflux for 4 h with stirring under the protection of nitrogen atmosphere. Then the yellow precipitate was collected by filtration, washed with diethyl ether and dried under vacuum. Yield was ~ 40%; elemental analysis calcd (%) for $C_{28}H_{22}N_4O_4$ (Mr = 478.16): C 70.28, H 4.63, N 11.71, O 13.37; found: C 73.20, H 4.95, N 10.35, O 12.50; ^{1}H NMR (DMSO): δ = 9.10 (dd, 4H), 8.92 (d, 2 H), 7.79 (dd, 4H), 7.72 (d, 2H), 7.13 (dd, 2H), 7.12 (dd, 2H), 3.83 (s, 6H) ppm; ESI-MS: m/z 479.02 [M^+]; FTIR: 3420 cm^{-1} (-OH), 3080 cm^{-1} (=CH), 1616.5 cm^{-1} (C=N phen), 1565.3 cm^{-1} (C=N imines), 1253.3 cm^{-1} and 1072.7 cm^{-1} (OCH_3).

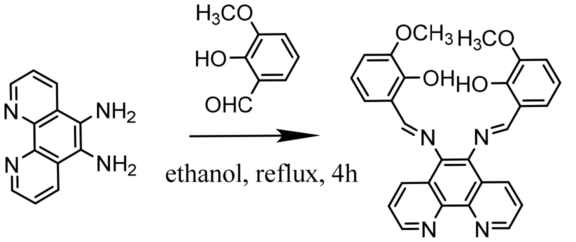

Synthesis of Co-PBI [Co^{II}-(phenbisimino-Co^{II})$_2$]. The method is according to the reference:[2] the above synthesized salenphen ligand (PBI, 60 mg, 0.125mmol) was dissolved into 20 mL ethanol and 47 mg (0.19 mmol) cobalt acetate tetrahydrate was added in the solution. The mixture was then heated at 70 ℃ for 2 hours with stirring till brown precipitate produced. After cooling, the product was filtered, washed with ethanol and diethyl ether. Finally, dry it in the vacuum overnight. Yield was ~ 35 %; elemental analysis calcd (%) for $C_{60}H_{46}N_8O_{12}Co_3$ (Mr = 1247.1): C 57.73, H 3.69, N

8.98, O 15.39, Co 14.19; found: C 55.20, H 4.05, N 10.35, O 15.50, Co 14.90; ESI-MS: m/z 1188.29 [M^+ - (Ac)]; FTIR: 3080 cm^{-1} (=CH), 1625.1 cm^{-1} (C=N phen), 1568.1 cm^{-1} (C=N imines), 1253.0 cm^{-1} and 1073.5 cm^{-1} (OCH_3).

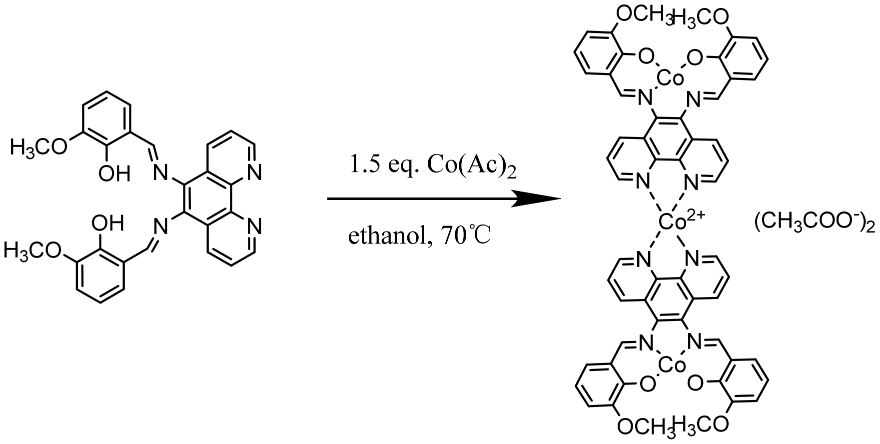

Synthesis Co-phen. 1,10-phenanthroline (50 mg, 0.25 mmol) and cobalt acetate tetrahydrate (32 mg, 0.125 mmol) were added in 20 mL ethanol, as well as heated to 60 ℃ for 2 hours.[3] The final product was filtered and washed by ethanol and diethyl ether. Yield was ~ 60 %; elemental analysis calcd (%) for $C_{28}H_{22}N_4O_4Co$ (Mr = 537.10): C 62.58, H 4.13, N 10.42, O 11.91, Co 10.97; found: C 65.20, H 4.05, N 8.35, O 12.50, Co 9.90; ESI-MS: m/z 477.80 [M^+ - (Ac)].

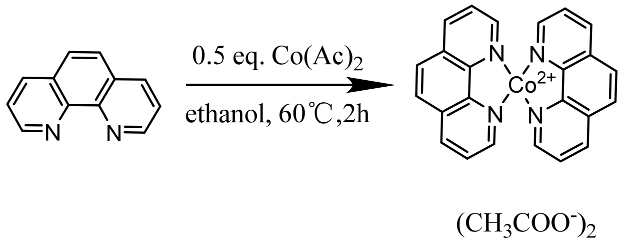

Synthesis Co-(phenbisimino)$_2$ (Co-P0). The method was modified from the above but exchanged the order of the steps. Firstly, the complex of bis(1,10-phenanthroline-5,6-diamine) cobalt (II) (Co-phenNH$_2$) was synthesized: 1,10-phenanthroline-5,6-diamine (116 mg, 0.5 mmol) and cobalt acetate tetrahydrate (63 mg, 0.25 mmol) were dissolved in 20 mL ethanol followed by the heating at 60℃ for 2 hours. Afterward, the first-step product was filtered and washed by the ethanol. Yield was ~ 50 %. Next the complex of Co-phenNH$_2$ (71 mg, 0.125 mmol) was added in the 20 mL ethanol containing 2-hydroxy-3-methoxybenzaldehyde (114 mg, 0.75 mmol) and 0.5 mL triethyl orthoformate. After reflux for 4 h with stirring under the nitrogen atmosphere, the product was formed and collected by the filtration. Yield was ~ 35 %. Elemental analysis calcd (%) for $C_{60}H_{50}N_8O_{12}Co$ (Mr = 1133.3): C 63.55, H 4.44, N 9.88, O 16.93, Co 5.20; found: C 65.2, H 5.1, N 9.4, O 16.1, Co 4.3; ESI-MS: m/z 1073.5 [M^+ - (Ac)]; FTIR: 3425 cm^{-1} (-OH), 3082 cm^{-1} (=CH), 1622.1 cm^{-1} (C=N phen), 1560.1 cm^{-1} (C=N imines), 1250.2 cm^{-1} and 1075.8 cm^{-1} (OCH_3).

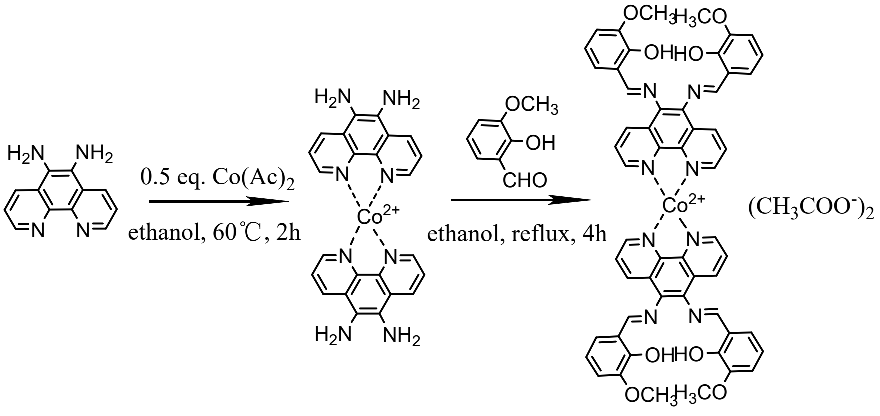

Synthesis of [N,N'-bis(salicylaldehyde)-1,2-phenylenediamine]cobalt (Co-salphen): The prepared method was followed as the previous reports.[4] Firstly, the ligand was produced: 1,2-benzenediamine (250 mg, 2.3 mmol) was dissolved in 15 mL ethanol together with 2-hydroxy-3-methoxybenzaldehyde (700 mg, 4.6 mmol). The solution was then refluxed at 70 ℃ for 2 hours until the orange precipitate (salphen) formation (yield: ∼ 80 %). After filtered and washed with ethanol, the precipitate was used to be reacted with cobalt. The salphen ligand (75 mg, 0.2 mmol) and cobalt acetate tetrahydrate (50 mg, 0.2 mmol) were dissolved in 20 mL ethanol followed by the heating at 60 ℃ for 2 hours. The generated dark yellow precipitate was filtered and washed by diethyl ether. Yield was ∼ 70 %. Elemental analysis calcd (%) for $C_{26}H_{24}CoN_2O_8$ (Mr = 433.1): C, 60.98, H, 4.19; Co, 13.60; N, 6.46; O, 14.77; found: C 58.2, H 5.0, N 6.1, O 16.1, Co 14.6. ESI-MS: m/z 432.8(M^+).

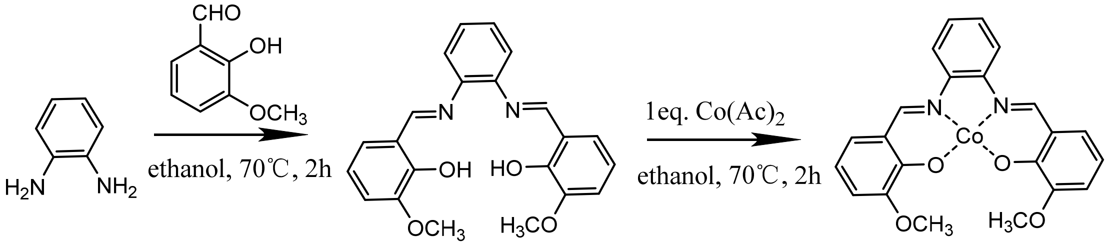

Synthesis of TiO_2 NR arrays. A typical hydrothermal method was used to prepare the TiO_2 NR arrays on a fluorine-doped tin oxide glass (FTO). Briefly, 0.2 ml titanium n-butoxide and 0.4 g NaCl were added into the 15 ml diluted hydrochloric acid (wt 18 %) and stirred until the mixture became clear. After that, the above solution was transferred into a 50 ml Teflon-lined autoclave where the FTO substrates were placed with the conductive side facing down. After 15 hours at 150 ℃, the FTO was washed with deionized water and dried in the air. Finally, the electrode was annealed at 550 ℃ for 2 hours.

Synthesis of hematite photoanode: According to previous studies,[5, 6] Fe_2O_3 was hydrothermally grown on the FTO glass (the conductive side faces down) in an aqueous solution with 0.15 M ferric chloride, and 1 M sodium nitrate. The autoclave was then transferred into a regular oven and kept at 100 °C for 24 h. The obtained yellow film of FeOOH on FTO was washed with distilled water and dried, after which it was annealed at 750 °C for 5 min for the generation of hematite.

Synthesis of photoanode@Co-PBI. The ligands and complexes grown on the TiO_2 were all prepared at the room temperature. In the first step, ligand PBI (60 mg, 0.125 mmol) was dissolved into 20 mL ethanol and an FTO glass with TiO_2 NRs was immersed in the solution for 2 hours to produce TiO_2@P1. The next step involves the TiO_2@P1 was transferred to an ethanol solution with cobalt acetate tetrahydrate (50 mg, 0.2 mmol) for 1 hour, after which the electrode was washed and dried to obtain TiO_2@Co-P1. Afterwards, the above photoanode was immersed into the PBI solution and $Co(Ac)_2$ again, respectively, to yield TiO_2@Co-P2 and TiO_2@Co-PBI. Fe_2O_3@Co-PBI was prepared in the same process. For comparison, photoanode/Co-Pi was fabricated by photo-assisted electrodeposition with the total Coulomb of 10 μC cm^{-2}.[7]

Characterizations. ^1H NMR spectra in [D6] DMSO were recorded on Bruker 600 MHz NMR spectrometer (Germany). ESI-MS was obtained with Finnigan TSQ Quantum Ultra electrospray ionization mass spectrometer (Thermo Fisher, USA). IR spectra were recorded with Nicolet iS 50 Fourier transform infrared spectrometer (Thermo Fisher USA). Raman spectra were recorded on a LabRAM HR Raman microscope (Horiba, France) with a laser excitation wavelength of 532 nm. UV-Vis data were acquired using a UV3600 (Shimadzu, Japan) spectrometer. The element analysis of C, H, N was carried out on the elemental analyzer (Leeman Labs, USA) and the metal composition was detected on the inductively coupled plasma optical emission spectrometer (SPECTRO, Germany). In addition, we also used Hitachi S4800 scanning electron microscopy (Japan) to obtain the SEM images.

Electrochemical and photoelectrochemical measurements. All electrochemical tests were carried out at room temperature on a computer-controlled Autolab PGSTAT 128N potentiostat / galvanostat (Metrohm, Switzerland) with a glassy carbon electrode (GCE) or conductive fluorine-doped tin oxide glass as working electrode, Ag/AgCl as reference electrode and platinum foil as counter electrode. The data were calibrated to the normal hydrogen electrode (NHE) by adding 0.199 V to the potential measurements. The photocurrent densities were measured under simulated sunlight irradiation using a 500 W Xe lamp equipped with an AM 1.5G filter (CEAulight, China). Before testing, the incident light intensity was determined and controlled at 100 mW cm^{-2} by a digital photo-power meter. Besides, a cubic quartz cell was used for all photoelectrochemical measurements.

Photocatalytic water oxidation testing. The photocatalytic reaction was carried out in an parallel irradiation type quartz reactor. The photocatalytic reaction was performed by taking Co-PBI catalyst in 50 ml of an aqueous phosphate buffer solution (pH = 7.0) containing 1.0 mM $[Ru(bpy)_3]^{2+}$, 5.0 mM $Na_2S_2O_8$, for O_2 evolution. The solution was stirred with a magnetic stirrer and evacuated for 40 min to remove air completely by purging with nitrogen. A sunlight simulator equipped with a 300 W xenon lamp was used as the light source and an AM 1.5G filter was employed to simulate the solar irradiation (100 mW cm^{-2}). The amount of evolved oxygen was detected by a dissolved oxygen probe (PASCO, USA) and calculated according to the Henry Law.

Theoretical calculations. The geometric optimization was firstly carried out by the Perdew-Wang, 1991 (PW91) of functional for Generalized Gradient Approximation (GGA) in $DMol^3$ package.[8, 9] The Double Numeric with Polarization (DNP) basis set and a SCF energy tolarance of 10^{-5} were employed. Moreover, the Gibbs free energy calculation was carried out by the frequency analysis of the optimized structures, and the applied potential was corrected to the reversible hydrogen electrode (RHE) by the equation of ΔG (U, pH) = ΔG - 0.0592 pH - neU, where n is the number of electron transfer, U is the reversible potential.[10]

Additional electrochemical measurements of Co-PBI:

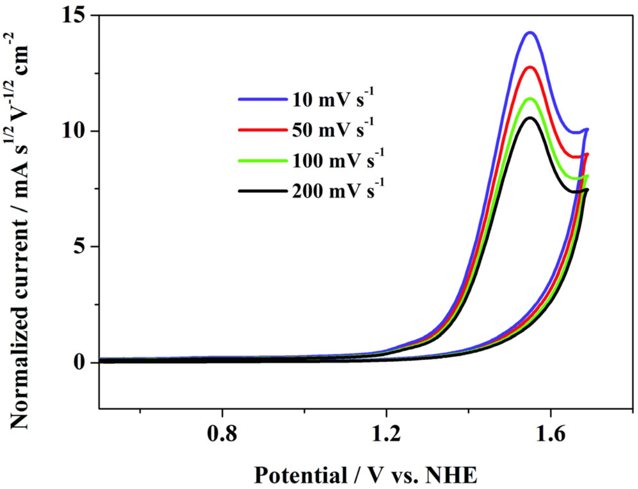

Fig. S1 CVs of the Co-PBI at different scan rates in the PBS (pH = 7.0).

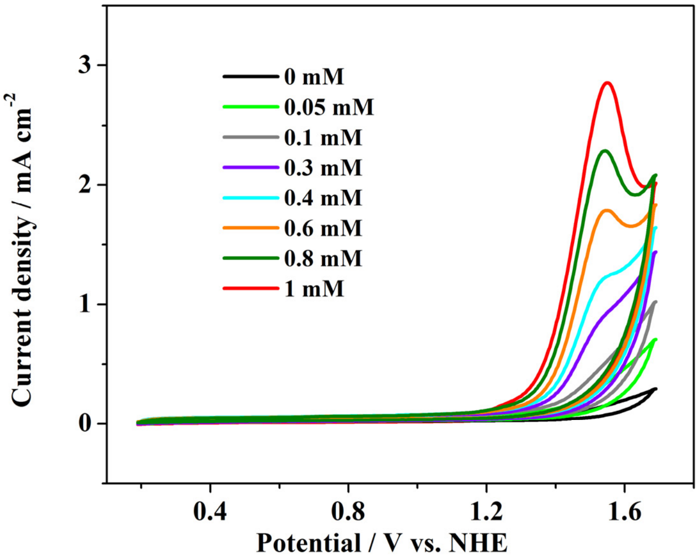

Fig. S2 CVs in the PBS with the addition of catalyst concentrations.

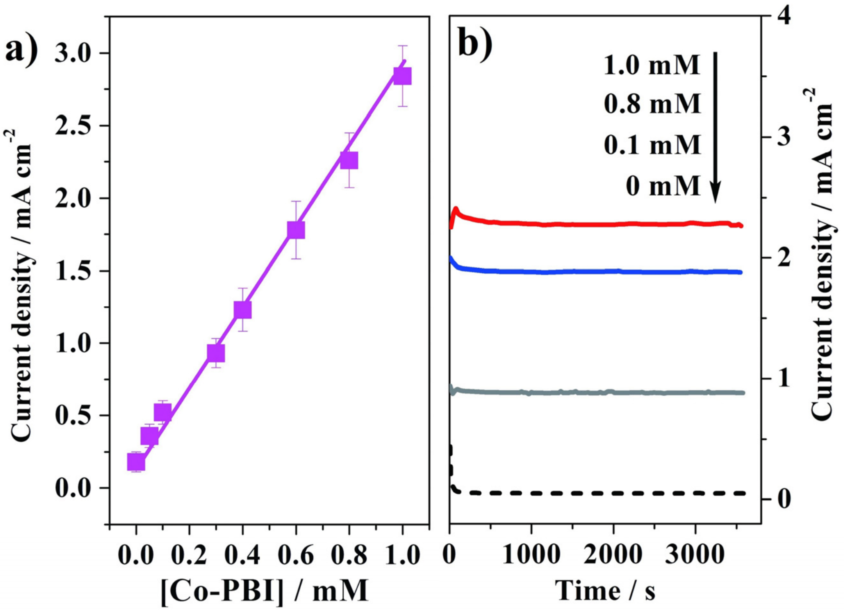

Fig. S3 a) The plots of the anodic current density versus the concentration of catalyst. **b)** Time-current density curves of the Co-PBI at 0, 0.1, 0.8 and 1.0 mM.

Investigation of homogeneous or heterogeneous catalysis in the neutral solution:

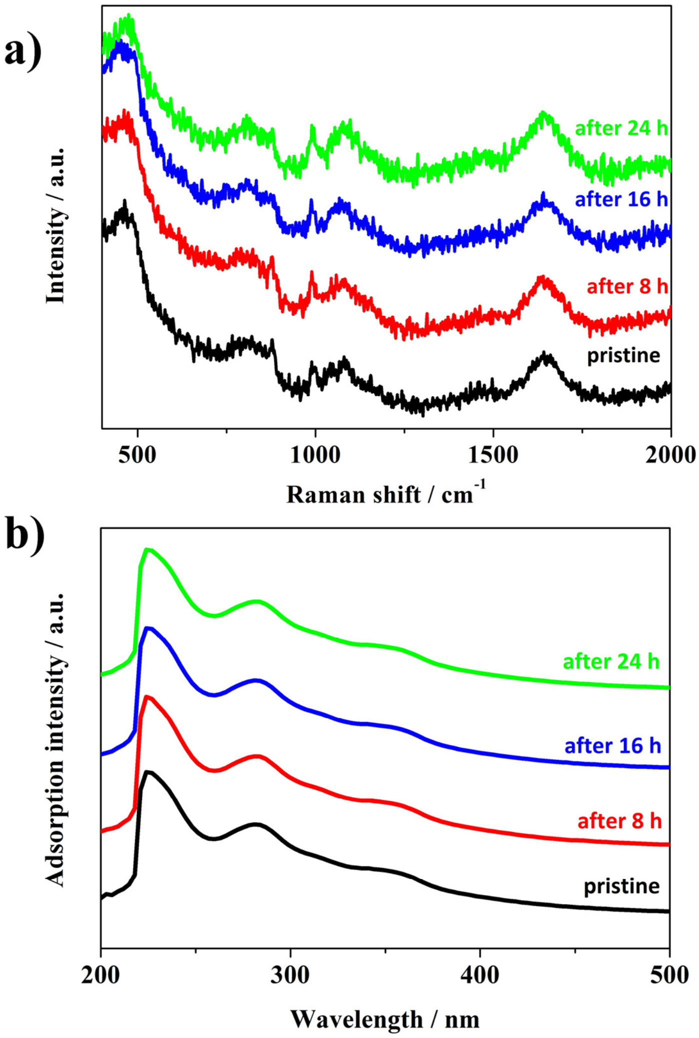

Fig. S4 (a) Raman and (b) UV-Vis spectra of the phosphate buffer solution containing Co-PBI before and after 8, 16, 24 h bulk electrolysis. No obvious change observed in the spectra reveals the macrocyclic structure of ligand is still remained after long-term electrolysis.

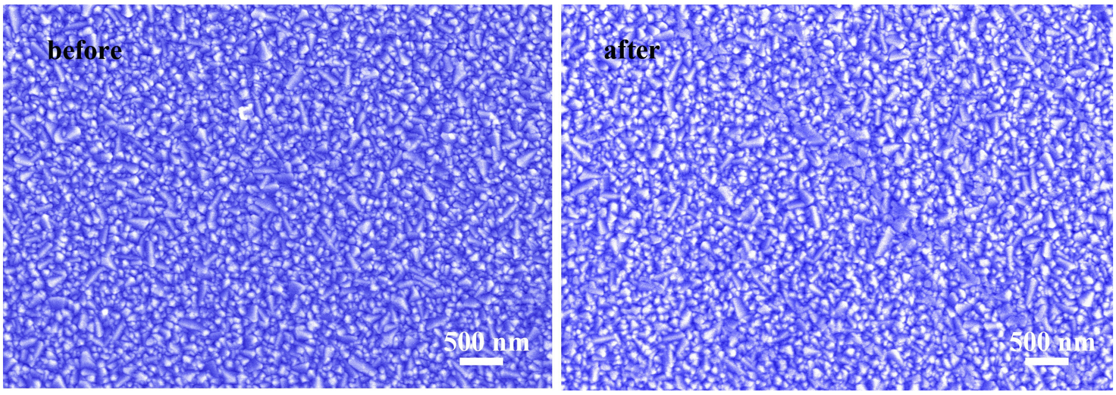

Fig. S5 SEM images of the surface of a FTO glass before and after electrolysis in PBS containing Co-PBI.

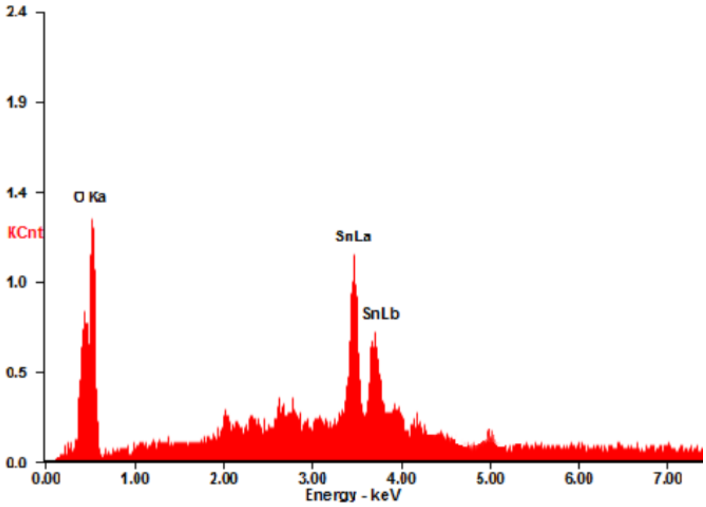

Fig. S6 EDX spectrum of the FTO glass after bulk electrolysis in Co-PBI.

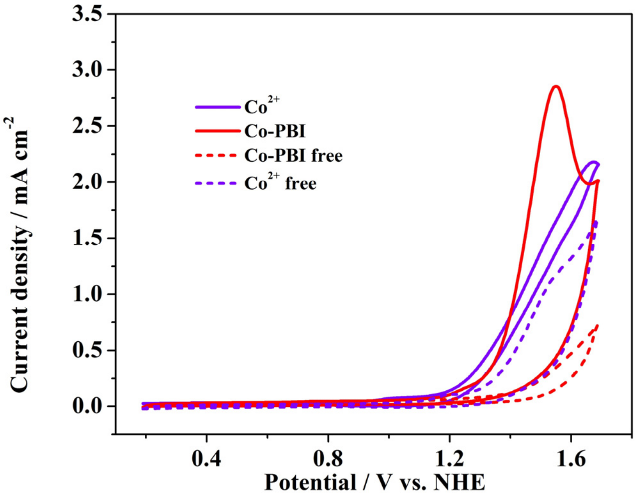

Fig. S7 CVs of GCE in 1.0mM Co-PBI or Co^{2+} (cobalt acetate) PBS solution (solid line). Afterward, the electrode after scanned 20 cycles is removed and washed by the deionized water (no polish); The other CVs are carried out on the electrode in the electrolyte without cobalt catalyst (dash line).

Co-Pi oxygen-evolving behavior is known as a typical heterogeneous electrocatalysis, distinguished from our prepared homogeneously catalytic complex. More specifically, the number of active sites for heterogeneous catalysts is almost several orders of magnitude more than that of homogeneous catalysts during water electrolysis. Therefore, the TOF of latter is much higher, supporting our results that Co-PBI shows TOF > 100 s^{-1}, while reported Co-Pi only exhibits 1.5×10^{-3} s^{-1}.(Energy Environ. Sci., 2011, 4, 499–504.) Although they illustrate closed potential and current density, the real kinetic parameters for them are quite different.

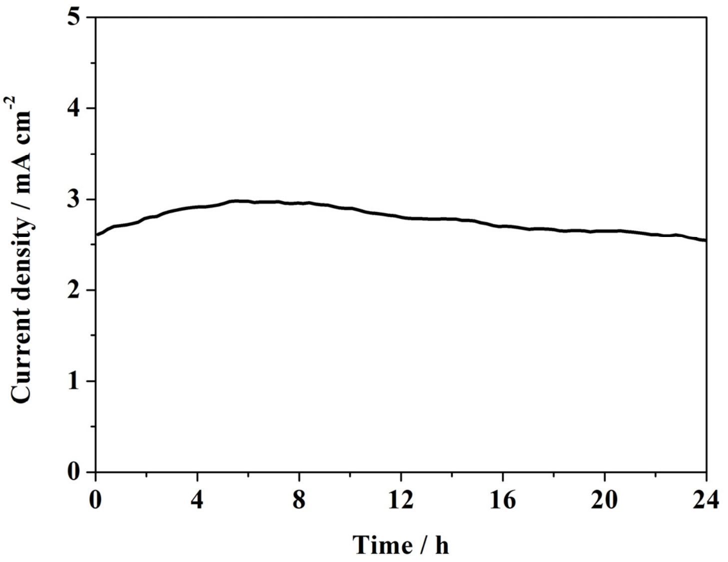

Fig. S8 Chronoamperometric study on Co-PBI in neutral solution at 1.5 V for 4 h.

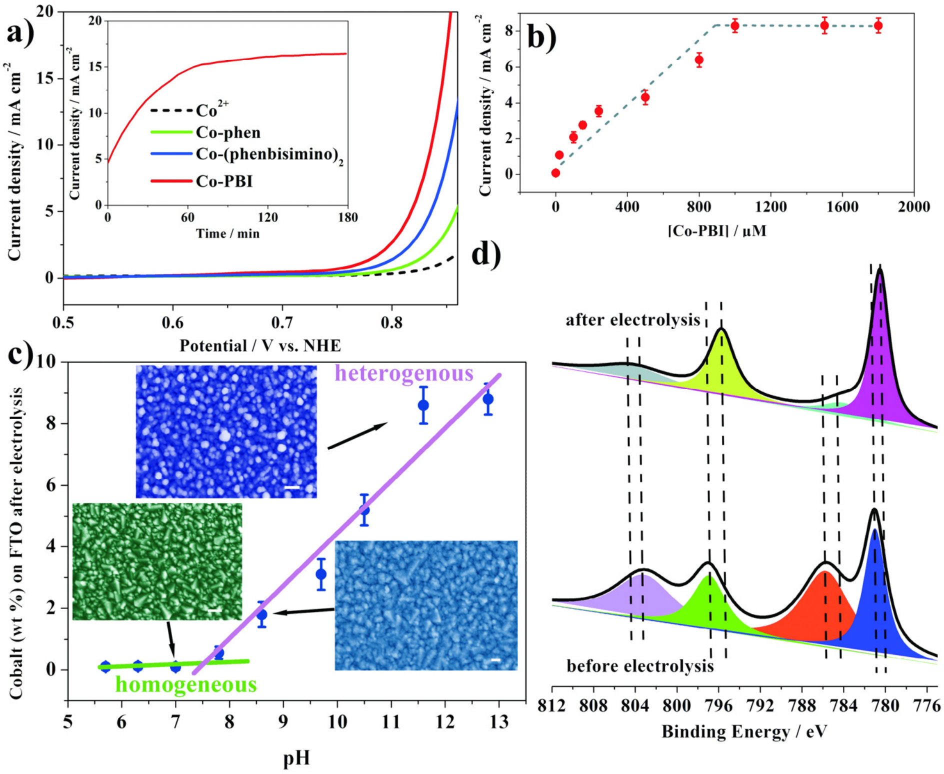

Fig. S9 a) Polarization curves of the glassy carbon electrode in the KOH electrolyte (pH = 12.8) containing 1.0 mM Co-PBI or 3.0 mM for others for controlling the same concentration of cobalt; the inset is the chronoamperometric response of the 1.0 mM Co-PBI. **b)** The plots of the anodic current density at 0.85 V versus the concentration of the Co-PBI in KOH. **c)** The transformation of the homogeneous to heterogeneous catalysis on Co-PBI with an increase in the pH. **d)** XPS spectra (Co 2p) of the synthesized Co-PBI complex (before electrolysis) and the CoO_x deposited in-situ on an FTO glass (after electrolysis).

Photocatalytic oxygen evolution testing:

To determine whether Co-PBI could act as a photocatalyst for light-induced water oxidation, we measured the oxygen-evolving performance in PBS (pH = 7.0) containing Co-PBI, $Ru(bpy)_3Cl_2$ and $Na_2S_2O_8$, which was irradiated by an AM 1.5G solar simulator. Specifically, $Ru(bpy_3)Cl_2$ is used as a photo-sensitized dye to absorb sunlight by exciting the charge from HOMO (highest occupied molecular orbital) to LUMO (lowest unoccupied molecular orbital). Afterwards, the generated photoelectron would be captured by the strong oxidant $Na_2S_2O_8$ (sacrificed reagent), during which the remained photoholes should be delivered to water for oxygen evolution. Otherwise, water oxidation reaction is kinetically onerous since a multi-proton and charge transfer is required. In this paper, an efficient oxygen-evolving catalyst is added into the water to accelerate the rate of photoholes transfer from dye to water, which is also known as a co-catalytic system. Fig. 3 shows the time-resolved O_2 amount observed with different concentrations of the catalyst. Oxygen evolved under irradiation, and the amount increased linearly for a period of ~ 2000 s. Afterward, the rate for the generation of gas is significantly slower. The inset displays the plots of the initial velocities (υ) of the oxygen evolution versus the concentration of Co-PBI. The linear relation reveals the turnover rate is closed when the concentration ranges from 0 to 100 μM. Thus, we have successfully applied our cobalt-based molecular complex to the visible-light driven water oxidation reaction, making the complex a promising PSII catalyst for efficient artificial photosynthesis.

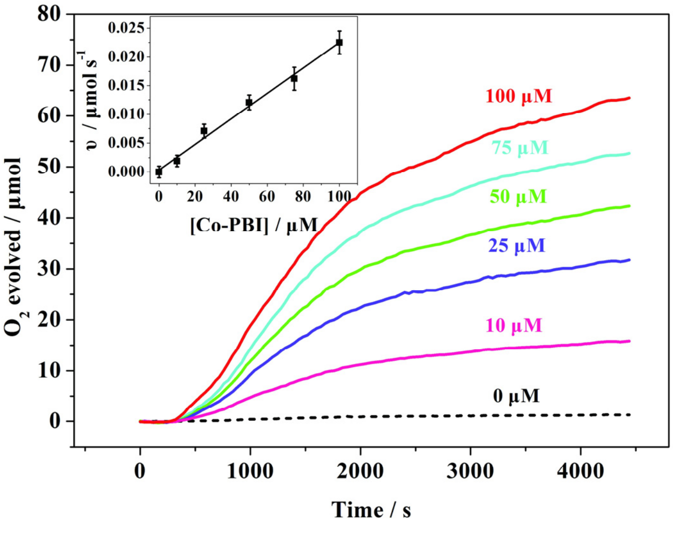

Fig. S10 Solar induced oxygen evolution from water for different concentrations of Co-PBI with 1.0 mM $[Ru(bpy)_3]^{2+}$ and 5.0 mM $Na_2S_2O_8$ in phosphate buffer solution.

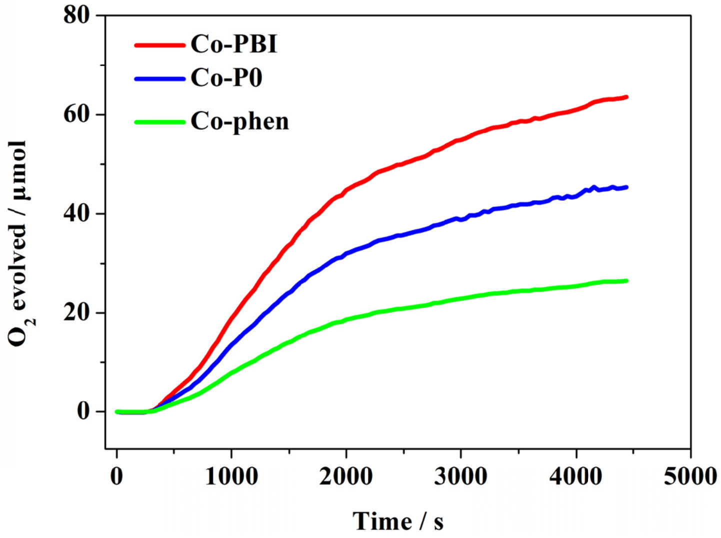

Fig. S11 Photocatalytic water oxidation performance of the three cobalt-based complexes; the concentration is 100 μM for Co-PBI and 300μM for other two.

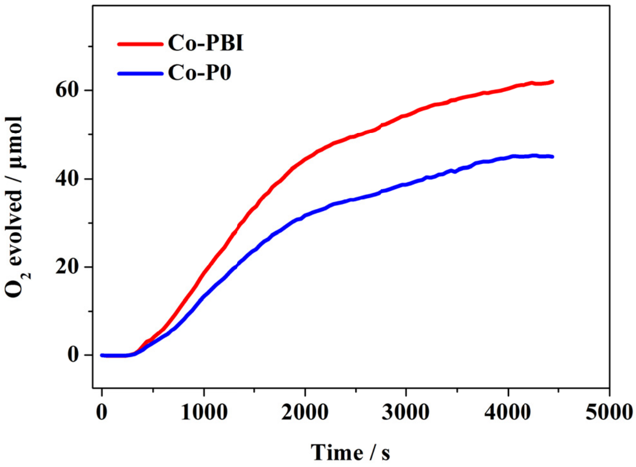

Fig. S12 Photocatalytic oxygen evolution from water for different concentrations of Co-PBI with 1.0 mM $[Ru(bpy)_3]^{2+}$ and 5.0 mM $Na_2S_2O_8$ in 0.1 M Na_2SO_4. The activity shows no decline compared with in the phosphate electrolyte, indicating the proton-acceptor is not necessary in the photochemical system.

Discussion of the distinctions between Co-PBI and Co-salphen:

We make an additional discussion here to supply some information of the importance regarding the presence of phen-cobalt center in the Co-PBI complex. Firstly, we conducted the CVs at full potential window of the three complexes, involving phen-Co only Co-P0 salen-Co only (Co-salphen) and both phen- and salen-Co (Co-PBI). Thus, it could be obvious to assign the redox peaks in the CVs as indicated in the Fig. S17. Specifically, the anodic waves for salen-Co are more negative than phen-Co, revealing the higher electrocatalytic activity of salen-Co for water oxidation. Moreover, the phen-Co center in Co-PBI also decrease the required potential of salen-Co$^{II/III}$ transformation contrasted with Co-salphen. The electrocatalytic water oxidation performance is also exhibited in the Fig. S18, where Co-PBI shows higher catalytic current density than Co-salphen at the equivalent concentration of cobalt. This could confirm that the central phen-Co in Co-PBI is also beneficial for OER. With the pH shifting to the alkaline region, we see Co-PBI holds higher activity than Co-salphen (Fig. S19). From our observation, the precipitate has formed in the solution of Co-salphen, which is not facilitated for the catalyst-to-electrode (diffusion) process. Moreover, attributing to the ionization of phen-Co, the Co-PBI demonstrates better solubility and improved diffused rate.

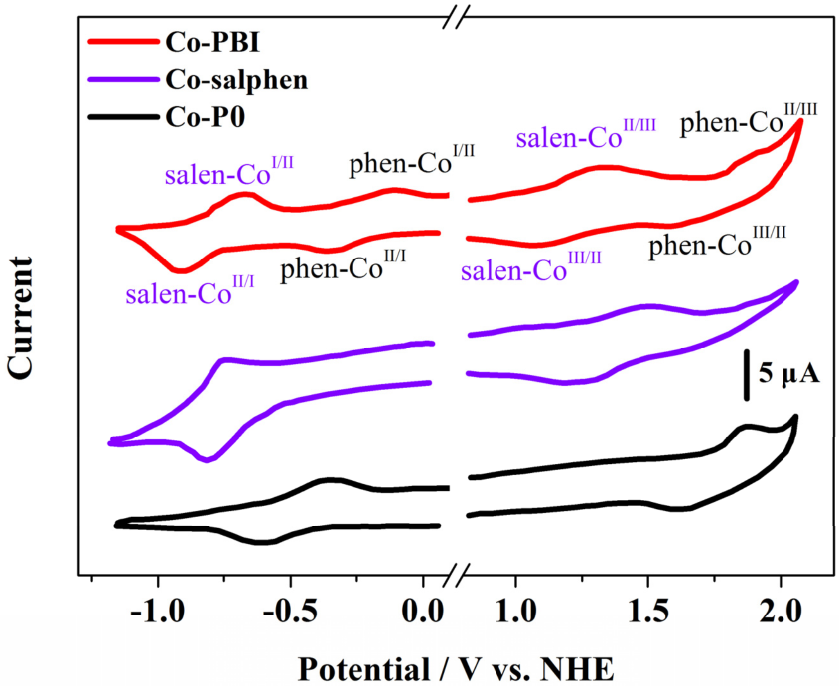

Fig. S13 CVs of the three complexes in the N,N-dimethylformamide (DMF) with 0.1 M 1-ethyl-3-methylimidazolium tetrafluoroborate (EMImBF$_4$) as supporting electrolyte. The scan rate is 10 mV s^{-1}, as well as the concentration of Co-PBI is 0.2 mM and the other two is 0.6 mM.

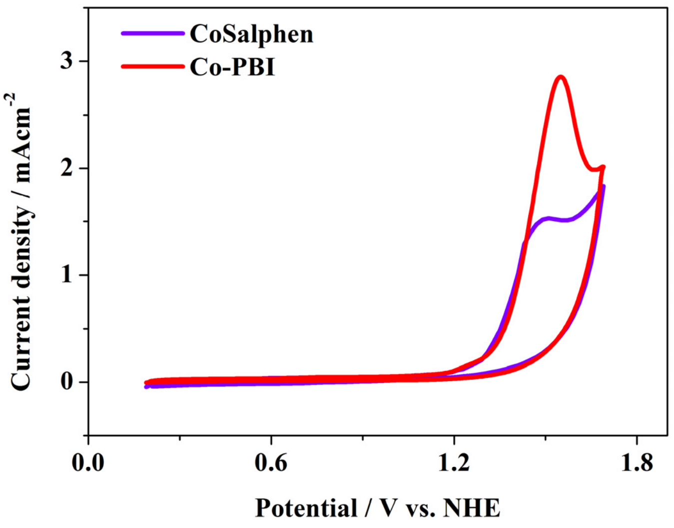

Fig. S14 CVs of Co-PBI and Co-salphen for water oxidation in 0.1 M phosphate buffer solution (pH = 7.0) with the same concentration of cobalt.

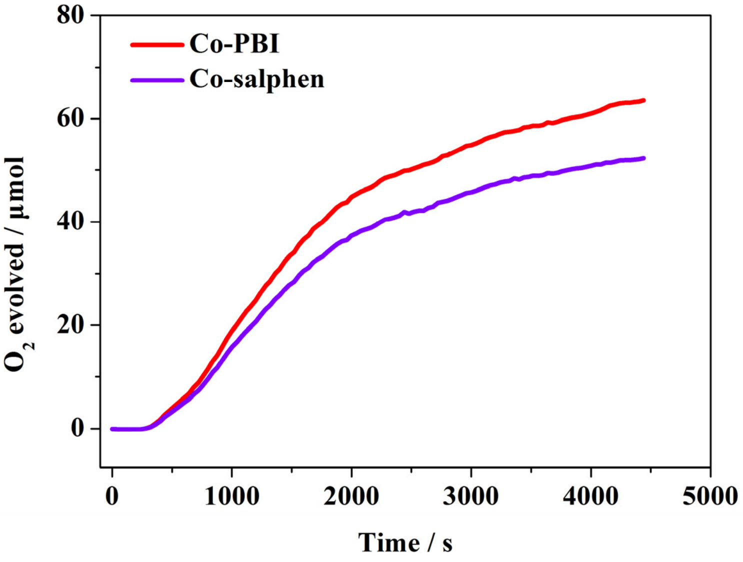

Fig. S15 Photocatalytic water oxidation performance on the two molecules (equivalent concentration of cobalt) in the neutral solution.

Table S1 Comparisons among reported homogeneous water oxidation electrocatalysts and Co-PBI in this work.

catalyst	**pH of electrolyte**	**catalyst concentration / mM**	**current density (@η= 0.7 V) / mA cm^{-2}**	**TOF / s^{-1}**	**reference**
copper-bipyridine	12.5	1.0	2.57	100	[11]
copper-polypeptide	11.0	0.9	3.14	33	[12]
$[Cu_2(BPMAN)(m\text{-}OH)]^{3+}$	7.0	1.0	0.5 (@η= 1.0 V)	0.6	[13]
macrocyclic nickel complex	7.0	1.0	1.14	-	[14]
manganese corrole complex	11.0	1.0	0.63	11.4	[15]
cobalt corrole complex	7.0	2.5 nmol cm^{-2} on ITO	0.15	0.2	[16]
dinuclear cobalt-polypyridine complex	7.0	0.5	1.14	-	[17]
cobalt porphyrins complex	7.0	1.0	1.0	-	[18]
Co-PBI complex	7.0	1.0	2.8	118	**this work**

Additional characterizations and PEC measurements:

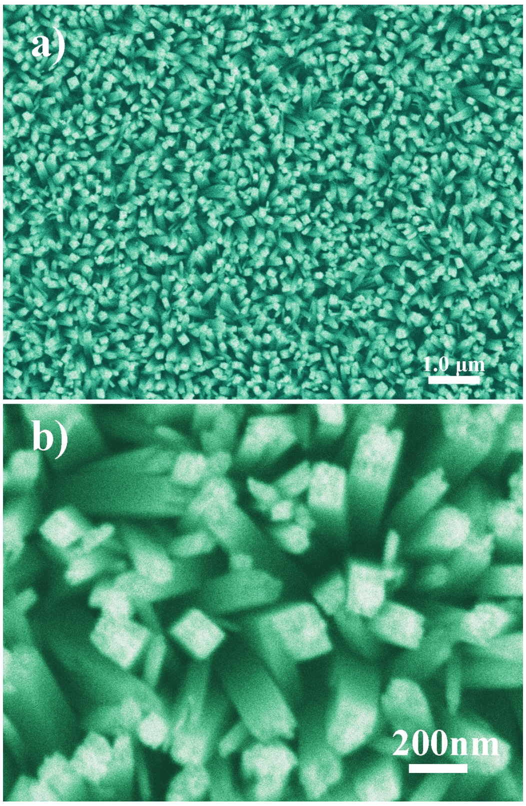

Fig. S16 SEM images of TiO_2 NR arrays on an FTO.

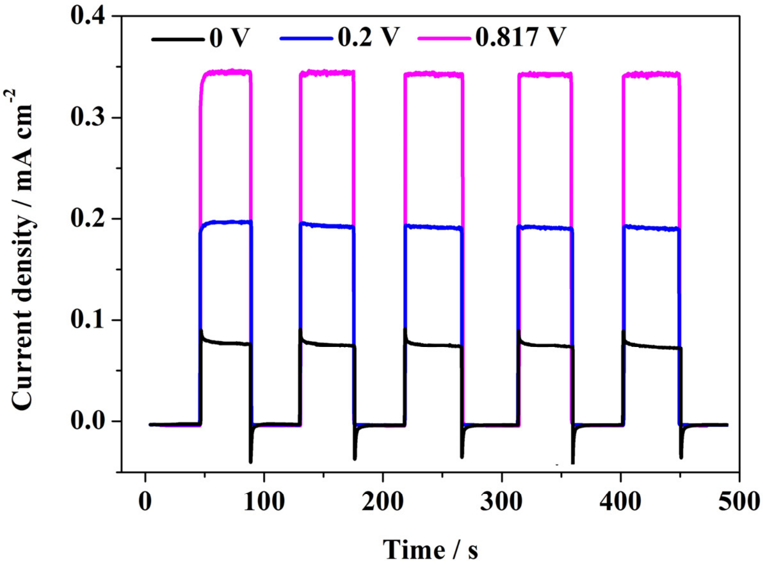

Fig. S17 Transient photocurrent density versus time for pristine TiO_2 NRs at 0, 0.2 and 0.817 V vs. NHE in phosphate buffer solution (pH = 7.0).

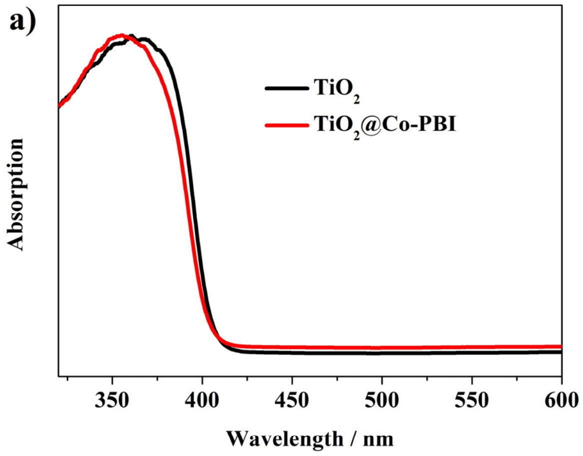

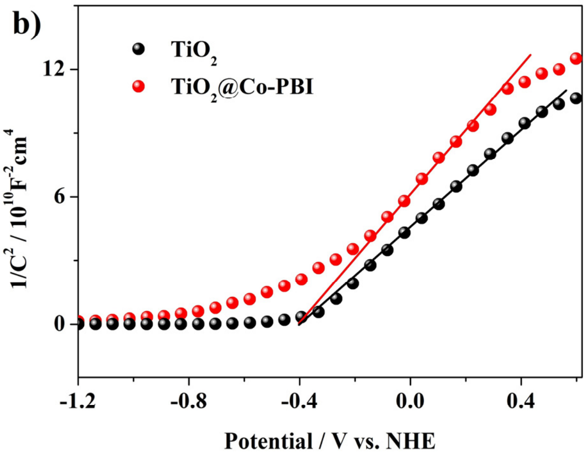

Fig. S18 a) UV-vis spectra of the pristine TiO_2 and TiO_2@Co-PBI photoanodes. b) Mott-Schottky plots of the pristine of TiO_2 and TiO_2@Co-PBI photoanodes collected at frequency of 5 kHz.

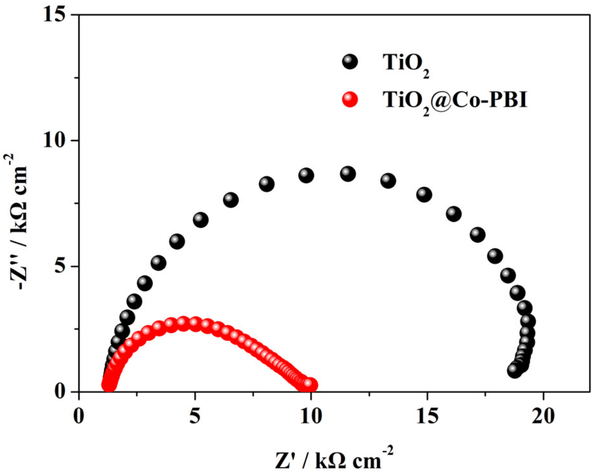

Fig. S19 Nyquist plots of TiO_2 with and without modified Co-PBI.

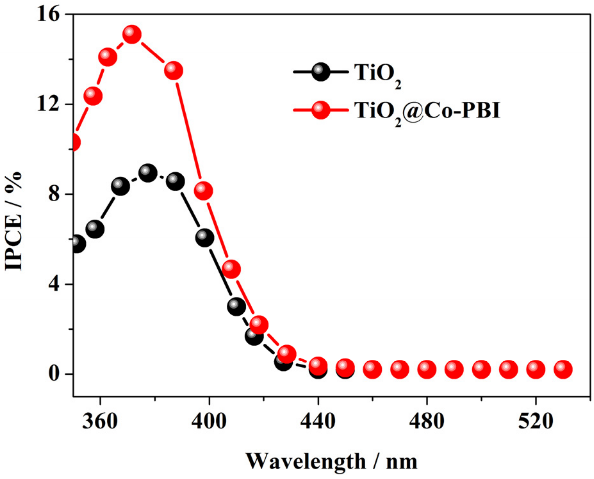

Fig. S20 IPCE determinations of TiO_2 with and without modified Co-PBI.

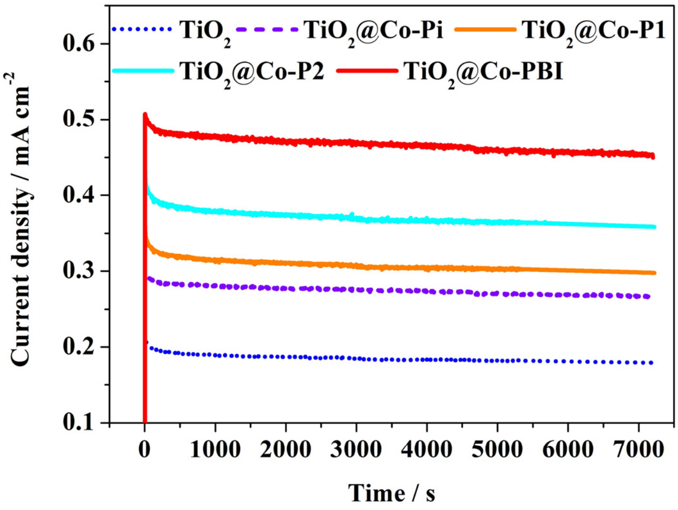

Fig. S21 Stability of photocurrent density for five photoanodes at a constant potential of 0.2 V vs. NHE.

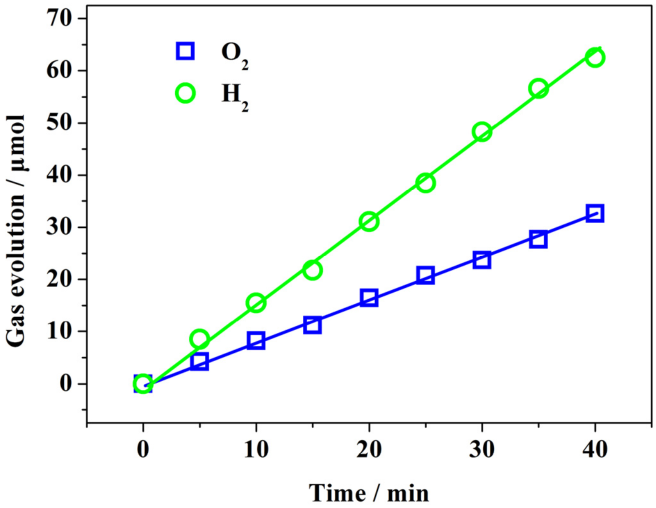

Fig. S22 Time-resolved hydrogen and oxygen evolution on the Pt and TiO_2@Co-PBI photoanode, respectively.

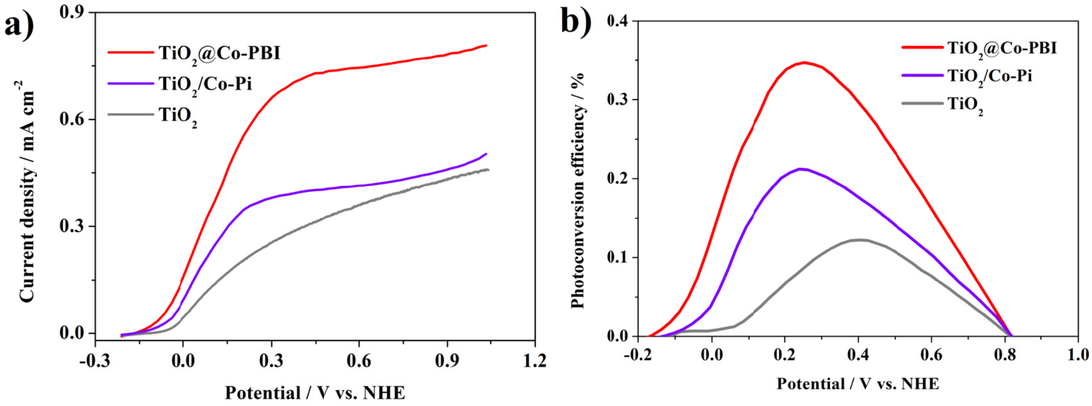

Fig. S23 **a)** Photocurrent versus potential measurements and **b)** corresponding calculated photoconversion efficiencies of TiO_2, TiO_2/Co-Pi, TiO_2@Co-PBI.

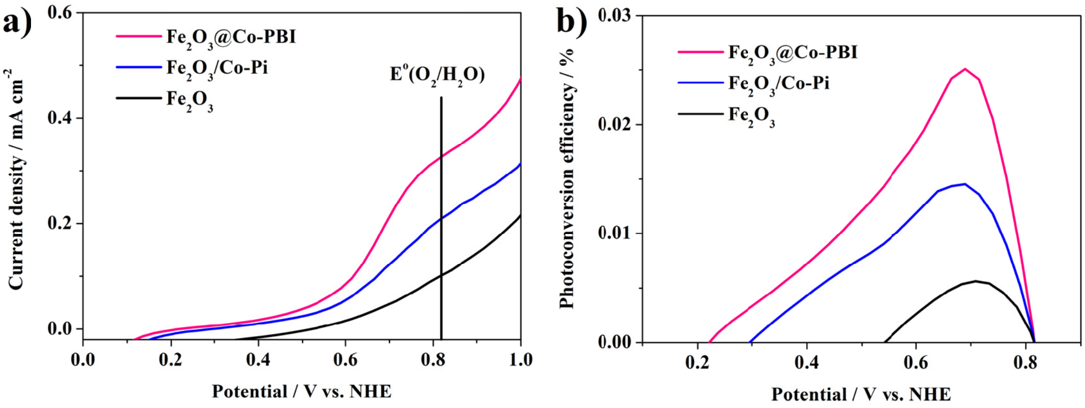

Fig. S24 **a)** Photocurrent versus potential measurements and **b)** corresponding calculated photoconversion efficiencies of Fe_2O_3, Fe_2O_3/Co-Pi, Fe_2O_3@Co-PBI. Hematite photoanode was prepared by the typical hydrothermal method followed with annealed in air.

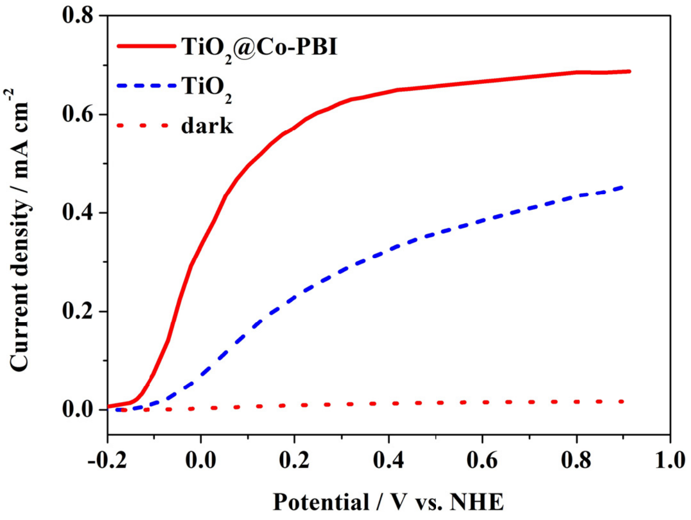

Fig. S25 Polarization curves of the photoanodes under irradiation or in dark in the electrolyte of 0.1 M Na_2SO_4.

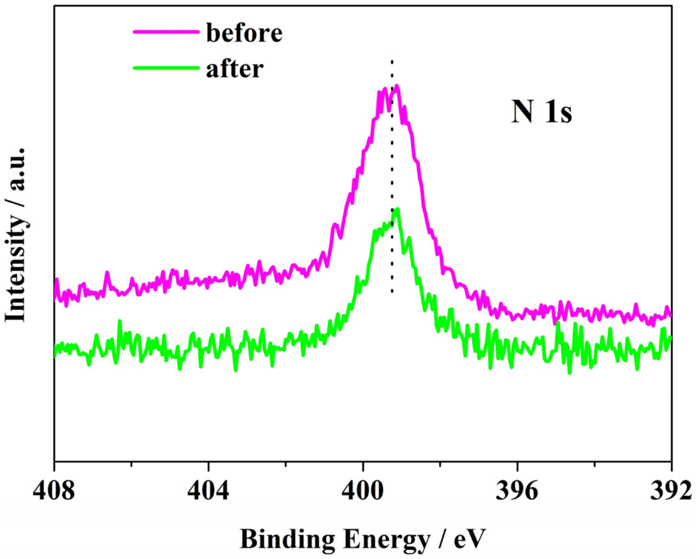

Fig. S26 XPS spectra of N 1s in TiO_2@Co-PBI before and after PEC measurements, in which there is no obvious change on binding energies. The peak at ~ 399.2 eV, the nitrogen in aromatic heterocyclic ring, is still observed after catalysis, implying the stability of Co-PBI.

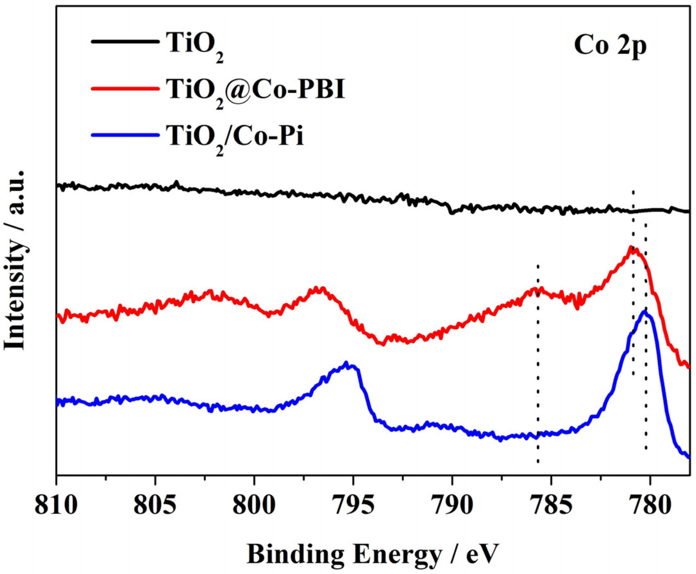

Fig. S27 XPS spectra of Co 2p in TiO_2@Co-PBI, TiO_2/Co-Pi, pristine TiO_2.

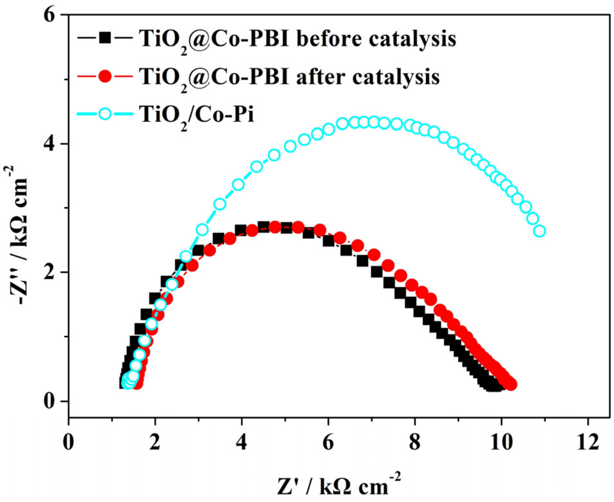

Fig. S28 EIS spectra of TiO$_2$@Co-PBI before and after PEC measurements ,compared with TiO$_2$/Co-Pi.

References:

1 P. P. Li, Z. Y. Jin, M. L. Zhao, Y. X. Xu, Y. Guo and D. Xiao, *Dalton Trans.*, 2015, **44**, 2208-2216.

2 N. Demirhan, U. Avciata and A. Gul, *Indian J. Chem. A*, 2005, **44**, 729-732.

3 F. A. Westerhaus, R. V. Jagadeesh, G. Wienhofer, M. M. Pohl, J. Radnik, A. E. Surkus, J. Rabeah, K. Junge, H. Junge, M. Nielsen, A. Bruckner and M. Beller, *Nat. Chem.*, 2013, **5**, 537-543.

4 E. Pizzolato, M. Natali, B. Posocco, A. M. Lopez, I. Bazzan, M. Di Valentin, P. Galloni, V. Conte, M. Bonchio, F. Scandola and A. Sartorel, *Chem. Commun.*, 2013, **49**, 9941-9943.

5 S. Shen, J. Zhou, C.-L. Dong, Y. Hu, E. N. Tseng, P. Guo, L. Guo and S. S. Mao, *Sci. Rep.*, 2014, **4**, 6627.

6 W. Li, S. W. Sheehan, D. He, Y. He, X. Yao, R. L. Grimm, G. W. Brudvig and D. Wang, *Angew. Chem. Int. Ed.*, 2015, **54**, 11428-11432.

7 G. J. Ai, R. Mo, H. X. Li and J. X. Zhong, *Nanoscale*, 2015, **7**, 6722-6728.

8 B. Delley, *J. Chem. Phys.*, 1990, **92**, 508-517.

9 B. Delley, *J. Chem. Phys.*, 2000, **113**, 7756-7764.

10 B. Hinnemann, J. K. Norskov and H. Topsoe, *J. Phys. Chem. B*, 2005, **109**, 2245-2253.

11 S. M. Barnett, K. I. Goldberg and J. M. Mayer, *Nat. Chem.*, 2012, **4**, 498-502.

12 M.-T. Zhang, Z. Chen, P. Kang and T. J. Meyer, *J. Am. Chem. Soc.*, 2013, **135**, 2048-2051.

13 X.-J. Su, M. Gao, L. Jiao, R.-Z. Liao, P. E. M. Siegbahn, J.-P. Cheng and M.-T. Zhang, *Angew. Chem. Int. Ed.*, 2015, **54**, 4909-4914.

14 M. Zhang, M.-T. Zhang, C. Hou, Z.-F. Ke and T.-B. Lu, *Angew. Chem. Int. Ed.*, 2014, **53**, 13042-13048.

15 W. Schöfberger, F. Faschinger, S. Chattopadhyay, S. Bhakta, B. Mondal, J. A. A. W. Elemans, S. Müllegger, S. Tebi, R. Koch, F. Klappenberger, M. Paszkiewicz, J. V. Barth, E. Rauls, H. Aldahhak, W. G. Schmidt and A. Dey, *Angew. Chem. Int. Ed.*, 2016, **55**, 2350-2355.

16 H. Lei, A. Han, F. Li, M. Zhang, Y. Han, P. Du, W. Lai and R. Cao, *Phys. Chem. Chem. Phys.*, 2014, **16**, 1883-1893.

17 H.-Y. Wang, E. Mijangos, S. Ott and A. Thapper, *Angew. Chem. Int. Ed.*, 2014, **53**, 14499-14502.

18 D. Wang and J. T. Groves, *Proc. Natl. Acad. Sci. U. S. A.*, 2013, **110**, 15579-15584.